Interactions between the Seasonal Cycle and El Niño–Southern Oscillation in an Intermediate Coupled Ocean–Atmosphere Model

PING CHANG AND LINK JI

Department of Oceanography, Texas A&M University, College Station, Texas

BIN WANG

Department of Meteorology, University of Hawaii, Honolulu, Hawaii

TIM LI

Atmospheric and Oceanic Science Program, Princeton University, Princeton, New Jersey

(Manuscript received 15 July 1994, in final form 5 December 1994)

ABSTRACT

The nonlinear interactions between the seasonal cycle and El Niño–Southern Oscillation (ENSO) in the coupled ocean–atmosphere system are examined using a newly developed intermediate coupled ocean–atmosphere model. The model permits coupling between total sea surface temperature (SST) and total surface winds and thus is able to produce its own seasonal cycle. This coupling approach allows for the examination of full dynamic interactions between the seasonal cycle and interannual oscillations. Numerical simulations with realistic surface heat fluxes indicate that this model is capable of capturing the essential variability of the coupled ocean–atmosphere system on seasonal-to-interannual timescale in the tropical Pacific.

Model sensitivity experiments were carried out by independently varying the external forcing strength and coupling strength. These experiments reveal a very different behavior of the coupled system with and without the seasonal cycle. In the presence of the seasonal cycle, the coupled model, in response to changes in the model parameters, undergoes several transitions between periodic (frequency-locking) and chaotic states. Chaotic response is found as the forcing amplitude approaches the observed value. In contrast, in the absence of the seasonal cycle, varying model coupling strength produces neither frequency-locking nor chaos. The coupled system simply undergoes a Hopf bifurcation from a nonoscillatory state to a periodic state as the coupling strength increases. This result suggests that nonlinear interactions between the forced seasonal mode and the intrinsic ENSO mode of oscillation are crucial for the irregular behavior of the model ENSO cycle. The experiments also show that a biennial oscillation can be excited by seasonal forcing even when air–sea coupling is so weak that a self-sustaining oscillation does not exist in the coupled system. This implies that the biennial oscillation observed as a fundamental element of ENSO variability in the low-latitude eastern Indian and western Pacific sector could be a subharmonic resonant to the seasonal forcing rather than a self-sustaining oscillation of the coupled system. Analysis of SST time series further demonstrates that major ENSO "episodes" in the coupled model exhibit a preferred phasing with the seasonal cycle. This phase-locking with the seasonal cycle occurs not only when the model ENSO cycle is periodic but also when it is chaotic. However, phase locking in the model appears to be tighter than that in nature. This study uncovers dual roles of the seasonal cycle in ENSO variabilities: it introduces a degree of regularity into the ENSO cycle by producing annual phase-locking and it generates chaos in the coupled system through inherent nonlinear interactions.

1. Introduction

The existence of coupling between the seasonal cycle and the Southern Oscillation was long ago recognized by Gilbert Walker. In one of his classical papers on the subject (Walker and Bliss 1932), Walker studied the seasonality of the Southern Oscillation by computing seasonal correlation fields based on a limited number of observations. With an increase in availability of observations, the close linkage between the seasonal cycle and ENSO cycle has been firmly established by a series of more recent empirical studies (e.g., Rasmusson and Carpenter 1982; Ropelewski et al. 1988; Rasmusson et al. 1990). These studies have clearly demonstrated that El Niño–Southern Oscillation (ENSO) has a strong tendency for phase locking with the annual cycle. This annual phase locking, as pointed out by Rasmusson et al. (1990), introduces a degree of regularity into the ENSO cycle. However, in

Corresponding author address: Dr. Ping Chang, Department of

served time series records (Trenbenth and Shea 1987) indicates that the recurrence interval of ENSO varies between two and seven years. Gu and Philander (1995), using wavelet analysis, demonstrated that the amplitude of the ENSO cycle has changed considerably over the past century. The observational evidence points to the ENSO cycle as an aperiodic phenomenon, even though its rhythm may be oscillatory. The question now is what causes its irregularity.

Many ENSO modeling efforts are based on coupled ocean–atmosphere models that specify the seasonal cycle (Cane and Zebiak 1987; Anderson and McCreary 1985; Neelin 1989; Barnett et al. 1993) or that have no seasonal cycle (Philander et al. 1992; Lau et al. 1992). These models allow coupling only between sea surface temperature and surface wind anomalies. The oscillatory behavior of ENSO in these models can be understood as a delayed oscillator mechanism in which equatorially trapped waves play a crucial role in maintaining a continual oscillation of the system by delaying the oceanic response to local wind forcing (Suarez and Schopf 1988; Battisti and Hirst 1989; Cane et al. 1990; Philander et al. 1992). Although the delayed oscillator theory provides a plausible explanation for the oscillatory rhythm of the phenomenon, it fails to explain its irregular characteristics. Recently, three independent studies (Jin et al. 1994; Tziperman et al. 1994; Chang et al. 1994) have proposed that the irregular occurrence of ENSO may be viewed as a low-order chaotic process driven by the seasonal cycle. Jin et al. (1994) and Tziperman et al. (1994) showed that as the coupling strength of the system is increased, a transition to chaos occurs as frequency-locking resonance overlaps. Chang et al. (1994), on the other hand, demonstrated that the coupled system can also be very sensitive to changes in the external forcing conditions. They showed that as the forcing amplitude is gradually increased, the coupled system undergoes transitions between periodic and chaotic states due to nonlinear interactions between the seasonal cycle and interannual oscillations.

The present study is an extension of the recent work of Chang et al. (1994) and represents a contribution sensitivity studies, that the biennial component of ENSO variability in the low-latitude eastern Indian and western Pacific sector may be a subharmonic resonating with the seasonal forcing rather than a self-sustaining oscillation of the coupled system.

The arrangement of the paper is the following: section 2 gives a brief description of a newly developed intermediate coupled model, including a discussion of differences between this model and the existing intermediate coupled models. Section 3 describes the model climatology and the model ENSO cycle from the control experiment in which realistic surface heat flux is used. Section 4 presents results from three sets of numerical experiments in which the sensitivity of the model response to changes in both external forcing and internal coupling parameters is examined. Section 5 depicts SST time series analyses that reveal the existence of a strange attractor, the annual phase-locking of the model ENSO cycle, and the secular changes of annual and interannual variability in the model. Finally, section 6 summarizes the major conclusions and discusses implications of using with coupled general circulation models.

2. The intermediate coupled model

The coupled ocean–atmosphere model used in this study involves atmospheric and oceanic physics of intermediate complexity. The major difference between previous intermediate models (such as Cane and Zebiak 1985; Anderson and McCreary 1985) and the present model is in its atmospheric component. In the previous intermediate coupled models, the atmospheric component is driven by an anomalous heat source, which simulates interannual fluctuations of surface winds, but not the climatological variations. In the present model, the atmospheric component is redesigned to include both the climatological variation and the interannual fluctuations of the surface winds. Based on the observational evidence that the annual variation of the vertically averaged lapse rate plays an important role in determining sea level pressure, the simple atmospheric model first calculates the vertically averaged

pability of simulating not only interannual variations of the surface winds but also the climatological variations when forced with the observed total SST in the tropical Pacific (Li and Wang 1994).

The oceanic component is a Cane and Zebiak type of ocean model (CZ model hereafter) that has been used extensively in ENSO modeling studies. The model has an interface between two immiscible layers of fluid, each of constant density, which simulates the sharp and shallow tropical thermocline separating the warm surface waters from the cold waters of the deep ocean. The motion in the upper layer obeys the conservation laws for mass and momentum. The lower layer is assumed to be infinitely deep. To keep its kinetic energy finite implies that the lower layer is motionless. Embedded into this $1\frac{1}{2}$ reduced gravity ocean is a constant depth, linear Ekman layer to capture the intensity of wind driven surface currents and the associated vertical motion. The surface temperature is calculated using entrainment (upwelling) velocity computed from the divergence of the surface currents. This simple ocean model includes both the surface and the subsurface dynamics in a crude way. The model was originally developed to predict changes in anomalous SST and was coupled with an anomalous atmospheric model for ENSO simulation (Cane and Zebiak 1985; Zebiak and Cane 1987). It has been subsequently modified by Seager et al. (1988) and Chang (1994) to include surface heat flux forcing for predicting changes in total SST field. The version used here follows closely to that of Chang (1994), which includes a simple parameterization scheme for the subsurface temperature change given by $T_d = \bar{T}_{\text{sub}} + \delta\partial_z\bar{T}_{\text{sub}}(h - \bar{h})$, where $\bar{T}_{\text{sub}}$ and $\partial_z\bar{T}_{\text{sub}}$ are the observed subsurface mean temperature and its vertical derivative at 50 m, $h - \bar{h}$ is the model thermocline fluctuation from its mean value, δ is an adjustable parameter that controls influence of thermocline fluctuation on SST and thus determines the coupling strength between the model atmosphere and ocean. This coupling parameter is shown to be of great importance in determining interannual oscillation in the coupled system. In the following numerical experiments, δ is chosen as a varying parameter to examine the sensitivity of the coupled model response to changes in the coupling strength. Seager et al. (1988) and Chang (1994) have shown that the model is capable of capturing the essential seasonal SST variability in the tropical Pacific when forced with the climatological surface winds and heat flux forcing. A summary of the model equations and model parameters can be found in the appendix. A more detailed description of the ocean model physics and its numerical scheme are given in Chang (1994).

The atmospheric and oceanic components are coupled using a nonlinear relation between surface wind stresses and wind speeds, that is, $(\tau_x, \tau_y) = \rho_0 C_d |\mathbf{V}|(U, V)$, where C_d is a drag coefficient of value 1.3×10^{-3}, and $|\mathbf{V}|$ is the total wind speed. The external forcing of the model is prescribed from the monthly mean surface heat flux climatology of Esbensen and Kushnir (1981) (EK heat flux), which consists of the shortwave radiation, the longwave radiation, and the latent heat and sensible heat fluxes. The total surface heat flux Q is decomposed into six Fourier components so that their values at each time step can be precisely determined, namely, $Q = Q_m + A\sum_{n=1}^{6} Q_n$, where Q_m is the annual mean EK heat flux, Q_n is a Fourier component of seasonally varying EK heat flux, and A is an adjustable coefficient that controls strength of the seasonal heat flux forcing. To prevent the model from drifting from its climatological mean state in long-term integrations, a constant annual mean heat flux correction was used. Its value is determined by integrating the coupled model for 5 years with the annual mean surface heat flux plus a Newtonian damping term $-\gamma(T - T_{\text{mean}})$, where γ is taken to be $1/30$ day^{-1} and T_{mean} is the observed annual mean sea surface temperature. The domain of integration spans from 120°E to 80°W in longitude and from 30°S to 30°N in latitude with a resolution of 2° × 1°. A leapfrog scheme is used for time integration with a time step of 3 h.

3. The control experiment

In this section, we present results from a control experiment in which the observed surface heat flux is used to force the coupled model and the model coupling coefficient δ is set to be unity. Before the seasonal forcing is turned on, the coupled model is first forced with the observed annual mean surface heat flux with the heat flux correction. After five years of integration, the model reaches an equilibrium. Major observed features in the tropical Pacific, such as the warm pool of surface water in the western Pacific Ocean, the strong equatorial Ekman upwelling and the associated cold tongue in the eastern Pacific just south of the equator, the west-to-east shoaling thermocline along the equator, and the subtropical highs and near-equatorial trough of the atmospheric surface pressure and the associated southeasterly trade winds that cross the equator in the eastern Pacific are all reproduced realistically (not shown). The success in simulating the observed annual mean state was partly due to the flux correction used in the model forcing. However, this flux correction will not directly affect the model seasonal-to-interannual variabilities because it is kept as a constant in time after the model is spun up.

To simulate seasonal-to-interannual variations, the model integration was continued for 135 years with six Fourier components of EK heat flux added to the annual mean forcing plus the constant flux correction determined from the initial spinup run. In the tropical Pacific Ocean, the dominant signal of the seasonal fluctuations of sea surface temperature is in the eastern equatorial Pacific cold tongue region, particularly along the equator and the coast of South America. The SST

annual variations in this region are closely associated with the annual migration of the intertropical convergence zone (ITCZ). The amplitudes of the SST fluctuations in this region are comparable to those in the subtropical oceans. The SSTs are warmest on the equator during the boreal spring when the ITCZ is the farthest south and the equatorial trades are weakest. The joint effect of weak wind stress and strong surface heating minimizes vertical entrainment of the cold subsurface water and increases the temperature of surface water. In contrast, the SSTs are the coldest during the fall when the ITCZ is farthest north and the southeast trades are at their strongest near the equator. The cold surface water can be partially attributed to the enhanced vertical mixing due to the intensified surface wind stress through a positive feedback between the meridional wind and SST (Mitchell and Wallace 1992; Chang and Philander 1994). Figures 1a and 1b show the simulated climatology representing warm and cold seasons in April and October, respectively. The pronounced annual cycle of SST in the eastern Pacific is clearly captured by the coupled model. The amplitude of the SST annual cycle is particularly well simulated in the eastern Pacific cold tongue region, as illustrated in Fig. 2. However, it is also noted that there is a 1-month phase delay in the simulated SST annual cycle in comparison with the observations. This phase delay could be attributed to the uncertainty in the treatment of the surface heat fluxes in this region as shown by Chang

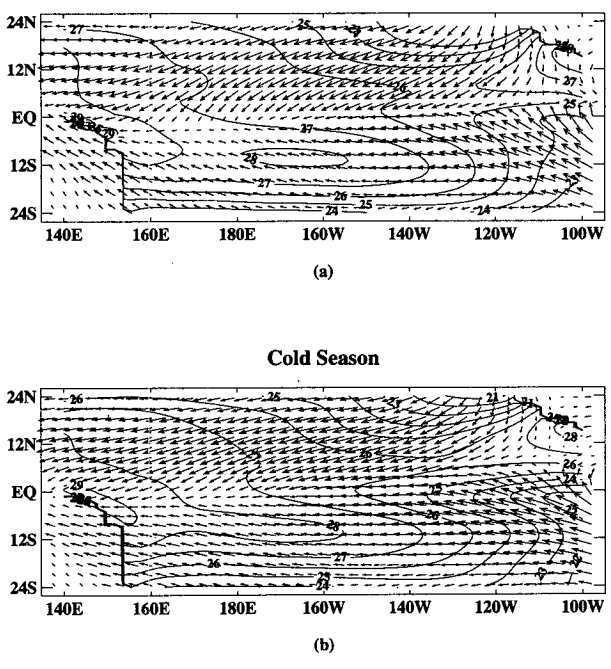

FIG. 1. Model climatological monthly mean SST and surface wind fields in (a) April and (b) October. The contour interval of SST is 1°C.

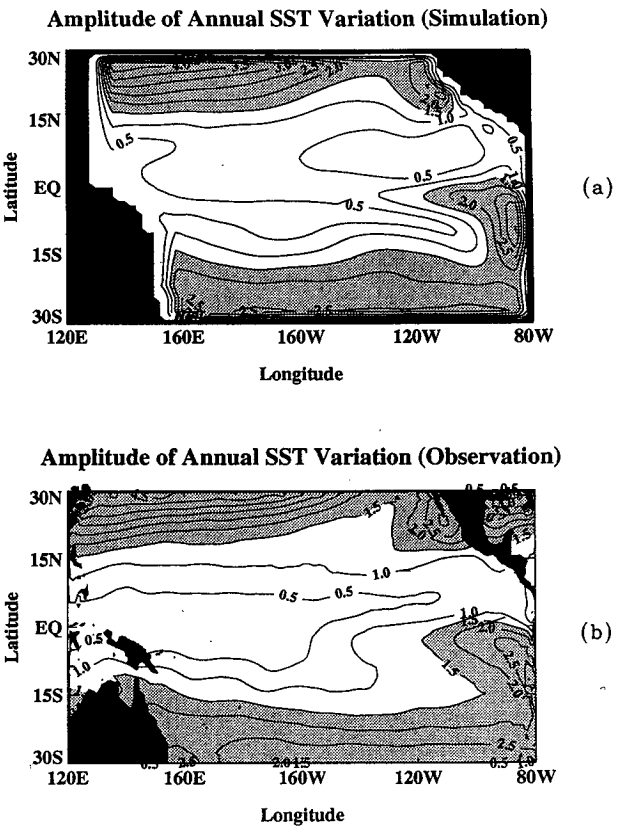

FIG. 2. Amplitude of annual SST variation from (a) the control experiment and (b) observations. The contour interval is 0.5°C and the regions where amplitudes are larger than 1.5°C are shaded.

(1994) and Wang et al. (1995). The other notable difference between the model simulation and observation is in the western Pacific warm pool region where the model SST is consistently too cold throughout the year when compared with observations, suggesting entrainment cooling may be overestimated by the simple ocean model. This difficulty in simulating warm pool temperature using the simple ocean model was previously noted by Chang (1994). In general, the coupled model gives a satisfactory description of the seasonal cycle in the tropical Pacific. The success of the simulation implies that the coupled model captures essential dynamics and thermodynamics governing the seasonal variation of the coupled tropical ocean and atmosphere system.

The model ENSO cycle in the control experiment is presented in terms of three dominant empirical orthogonal function (EOF) modes of SST anomaly (SSTA) derived from the last 100 years of the simulation. Figure 3 compares the three leading EOF modes from the simulated SSTA with those derived from observed SSTA. The observed SSTA field is derived from the Comprehensive Ocean and Atmosphere Data Set (COADS) during the period of January 1969 to De-

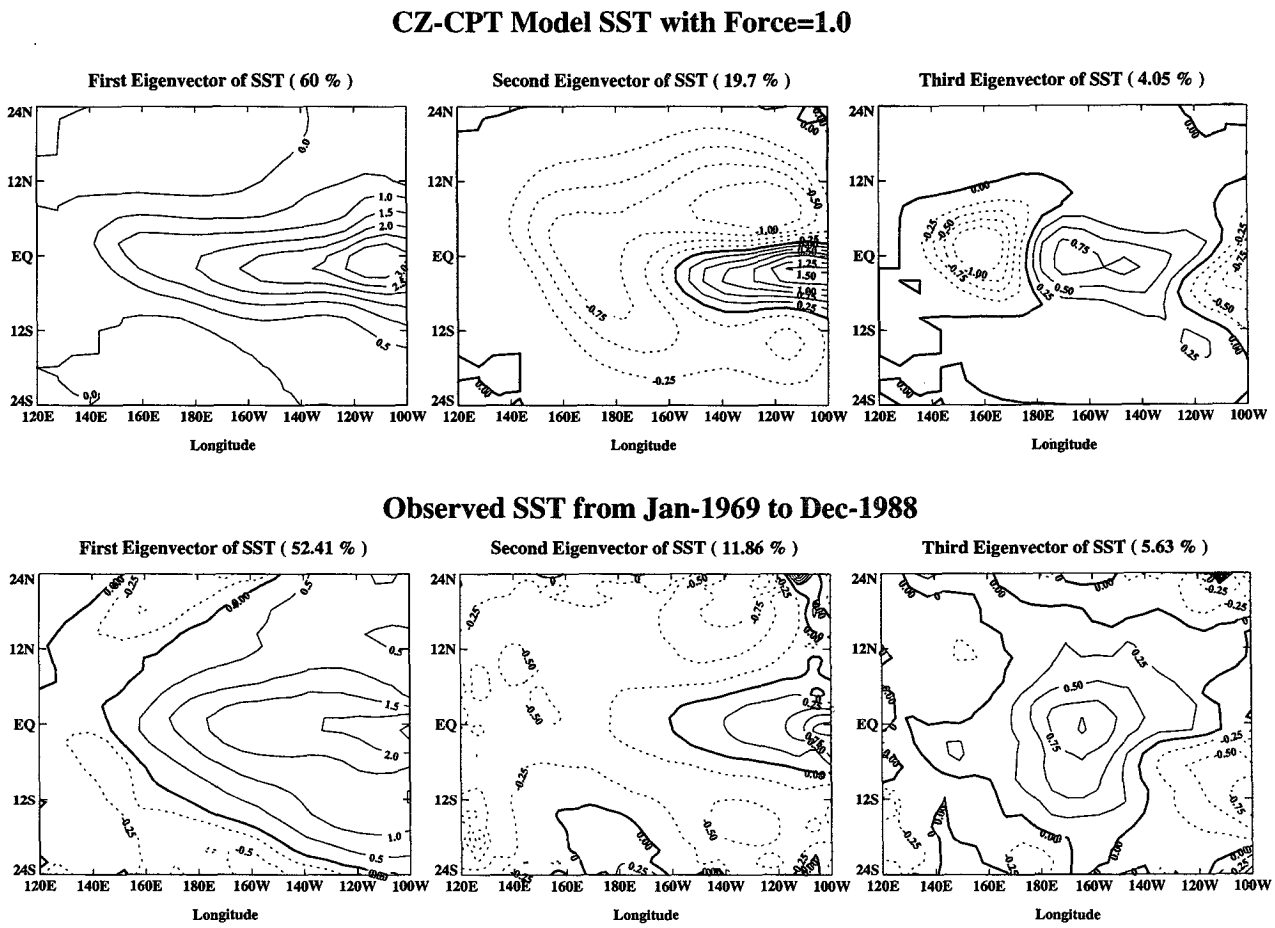

FIG. 3. First three leading EOFs of simulated SST anomaly (upper panel) and observed SST anomaly from COADS during January 1969 to December 1988. Contour interval is 0.5°C in the first EOFs and 0.25°C in the other EOFs.

cember 1988. The first three EOFs of the simulated SSTA account for 60%, 20%, and 4% of the total variance, respectively, which compares with 52%, 12%, and 6% of the total variance accounted for by the three leading modes from the observations. As seen in Fig. 3, the leading EOFs for simulated SSTA (Fig. 3, upper panel) bear a striking similarity to the observed modes, except that the simulated modes appear to be too narrowly confined near the equator. This narrow spatial structure of the model ENSO cycle is also noted in other intermediate coupled models (e.g., Cane 1993). An examination of the time series associated with the simulated EOF modes indicates that the second mode leads the first mode by approximately one month (not shown), suggesting that there is a westward propagating tendency for the SST anomaly along the equator in the model. Such a westward propagation of the SST anomaly is also observed in the ENSO episodes prior to the 1982–1983 event (Rasmusson and Carpenter 1982). Figure 4 shows the surface temperature anomalies and the corresponding surface wind anomalies for a "typical" warm and cold "ENSO episode" in the model. The anomalous equatorial trades are reasonably well captured by the coupled model when compared to the mature phase anomaly composite of major ENSO episodes compiled by Rasmusson and Carpenter (1982), except they are too confined meridionally and extend too far to the east. However, the wind anomalies in the eastern Pacific are unrealistically intense. This unrealistic feature in the anomalies wind fields is common to the Gill type of simple atmospheric models (Zebiak 1986), of which our model is a variation. Other unrealistic features include cold episodes that are too strong and warm episodes that last too long compared to the composite ENSO event. These shortcomings have been previously noted in other intermediate coupled models (Zebiak and Cane 1987; Battisti and Hirst 1989). Despite these shortcomings, major features of ENSO variability in the tropical Pacific are well captured by the intermediate coupled model.

In the following sections, we show that the model ENSO cycle in the control run exhibits strong irregularity. We further argue that the irregular behavior of model ENSO cycle in this case is governed by a low-

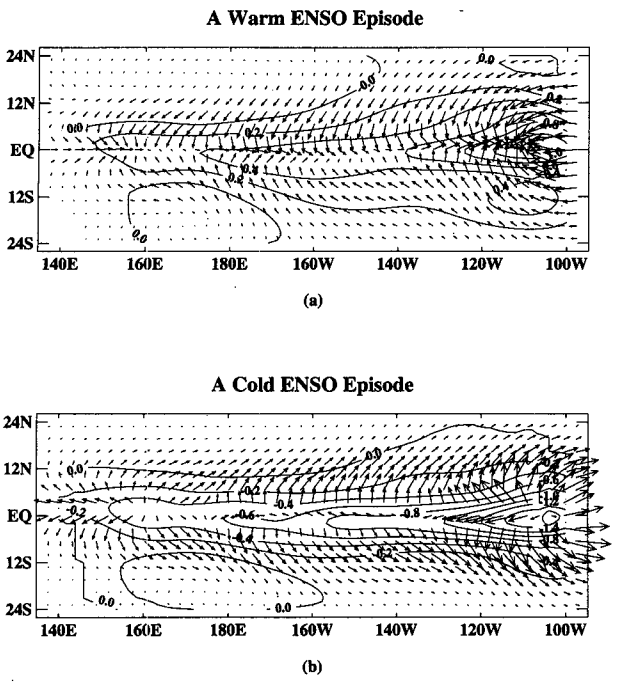

FIG. 4. SST and wind anomalies of (a) a "typical" warm ENSO episode and (b) a "typical" cold ENSO episode in the control experiment. Contour interval is 0.2°C.

order chaotic attractor and the chaos is caused by nonlinear interactions between the forced seasonal mode and the intrinsic ENSO mode of oscillation.

4. Sensitivity experiments: Frequency entrainment and chaos

To fully explore nonlinear interactions between the seasonal cycle and interannual oscillations in the coupled model, three sets of numerical experiments were conducted by independently varying the forcing amplitude parameter A and the coupling parameter δ. In the first set of experiments, the forcing amplitude parameter A is increased gradually from 0 to 1.5, while the coupling parameter δ is set to be unity. In the second set of experiments, the model seasonal cycle is removed by setting $A = 0$ and the coupling parameter δ is varied between 0.5 and 2. The third set of experiments are essentially the same as the second set except that the seasonal forcing amplitude is retained at its full strength by setting $A = 1$. Each simulation is integrated for 130 years and starts from an initial equilibrium state obtained by integrating the model for 5 years with the observed annual mean heat flux. The system is allowed to come to a steady state by omitting the first 40 driven cycles. The power spectrum analyses are performed on the monthly SST time series of the last 90 years model integration taken from 0°, 120°W in the model ocean, and phase portraits of SST are reconstructed using the daily SST time series. In the following subsections, we present results from each set of experiments with a more detailed discussion of the first set of experiments.

a. Experiments of varying forcing amplitude

Figure 5 shows SST power spectra of 24 different experiments selected from a total number of more than 70. Figure 6 shows nine selected SST phase portraits reconstructed using the method of time delays (Pachard et al. 1980). In the absence of seasonal forcing—that is, $A = 0$—the coupled model exhibits a regular, but nonsinusoidal oscillation with a period of 40 months. The SST power spectrum of SST (Fig. 5a) shows a fundamental frequency at $f_0 = 0.025$ (mo^{-1}) along with higher harmonics at integral multiples of this. Consistent with the power spectrum, the reconstructed SST phase portrait reveals a single period limit cycle. The leading EOFs (not shown) bear a close resemblance to the ones in the control experiment (Fig. 3, upper panel), except that the amplitudes are about 30% stronger. The physical mechanism responsible for maintaining the regular ENSO cycle of the model appears to be the "delayed-oscillator" studied extensively by a number of investigators (Suarez and Schopf 1988; Battisti and Hirst 1989; Cane et al. 1990).

When the forcing amplitude is small ($A < 0.025$), the seasonal cycle has little effect on the model ENSO cycle. The model maintains its regular oscillation with a period of 40 months. As the forcing amplitude is increased to above 0.025, the periodicity of the model ENSO cycle doubles and the power spectrum shows a peak at $f_0/2$ (Fig. 5b). Increasing the forcing amplitude causes the subharmonic peak at $f_0/2$ to grow until a second period doubling occurs when A reaches about 0.064 (Fig. 5c). Higher values of A lead to further bifurcations (Fig. 5d) and eventually to chaotic behavior at $A = 0.175$ (Fig. 5e). This route to chaos through a sequence of period doublings is illustrated in terms of phase portraits of the model SST (Fig. 6b–d). Each subharmonic bifurcation doubles the number of the period of limit cycles in the phase diagrams. The onset of nonperiodic oscillation is marked by broadband noise and broadened spectral peaks in the power spectra as shown in Fig. 5e. The reconstructed phase portrait shown in Fig. 6d depicts a chaotic orbit, suggesting the presence of a strange attractor.

As the forcing amplitude is further increased to above $A = 0.1875$, the model SST oscillation abruptly becomes regular again. However, the period of the oscillation shortens to 3 years (36 months) and the model ENSO frequency remains unchanged while the forcing amplitude is varied over a limited range of $0.1875 < A < 0.4$ (see Figs. 5f–h). This phenomenon is called frequency locking (or mode locking) and is known to be generally present in dissipative, nonlinear systems with competing frequencies (Bak et al. 1985). Within this frequency locking regime, the frequency ratio of the model ENSO cycle and annual cycle keeps

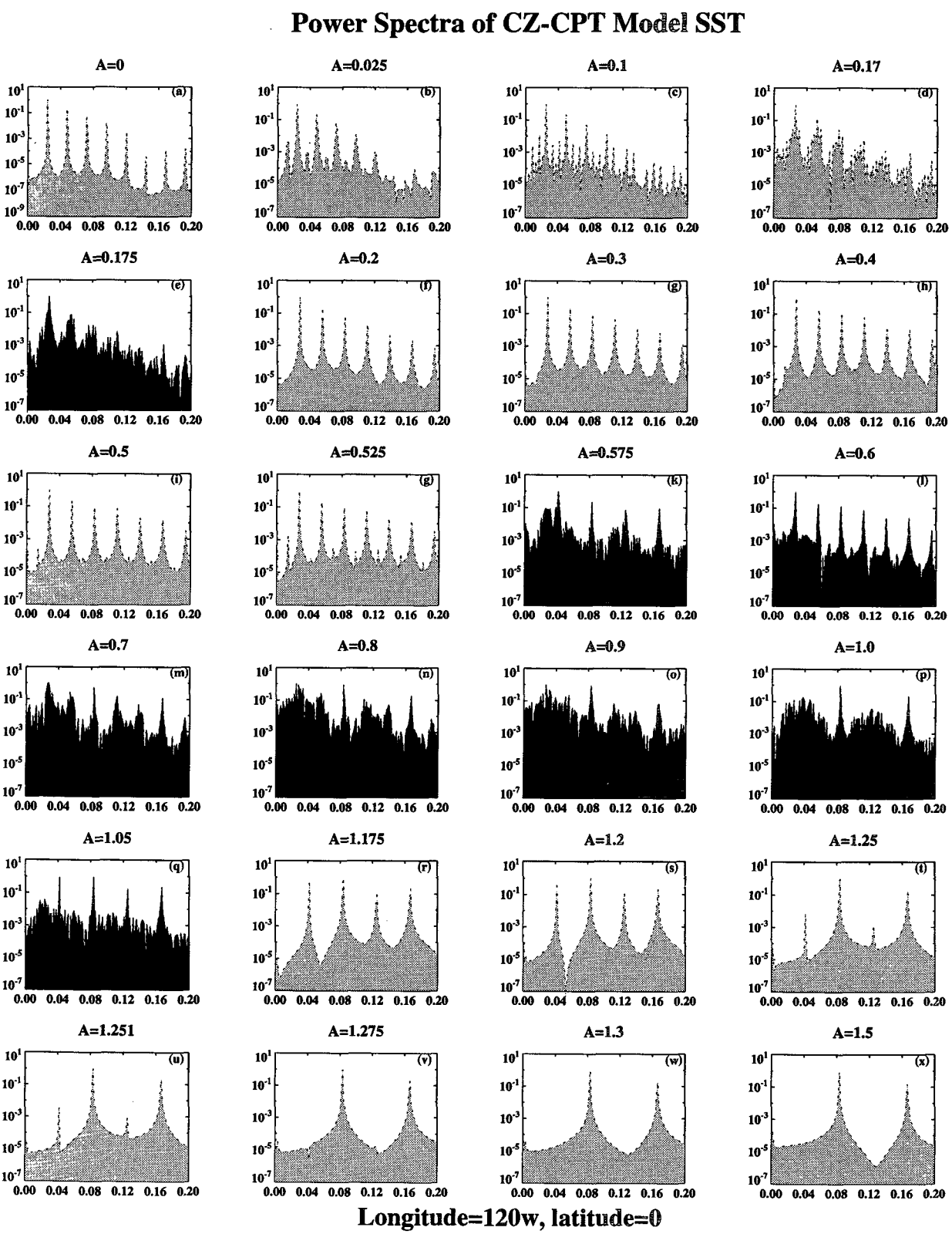

FIG. 5. Twenty-four selected power spectra of model SST time series at 0°, 120°W in the experiment where the seasonal forcing amplitude is increased from $A = 0$ to $A = 1.5$ from (a) to (x). The light shaded spectra correspond to periodic regimes and the dark shaded spectra indicate chaotic response.

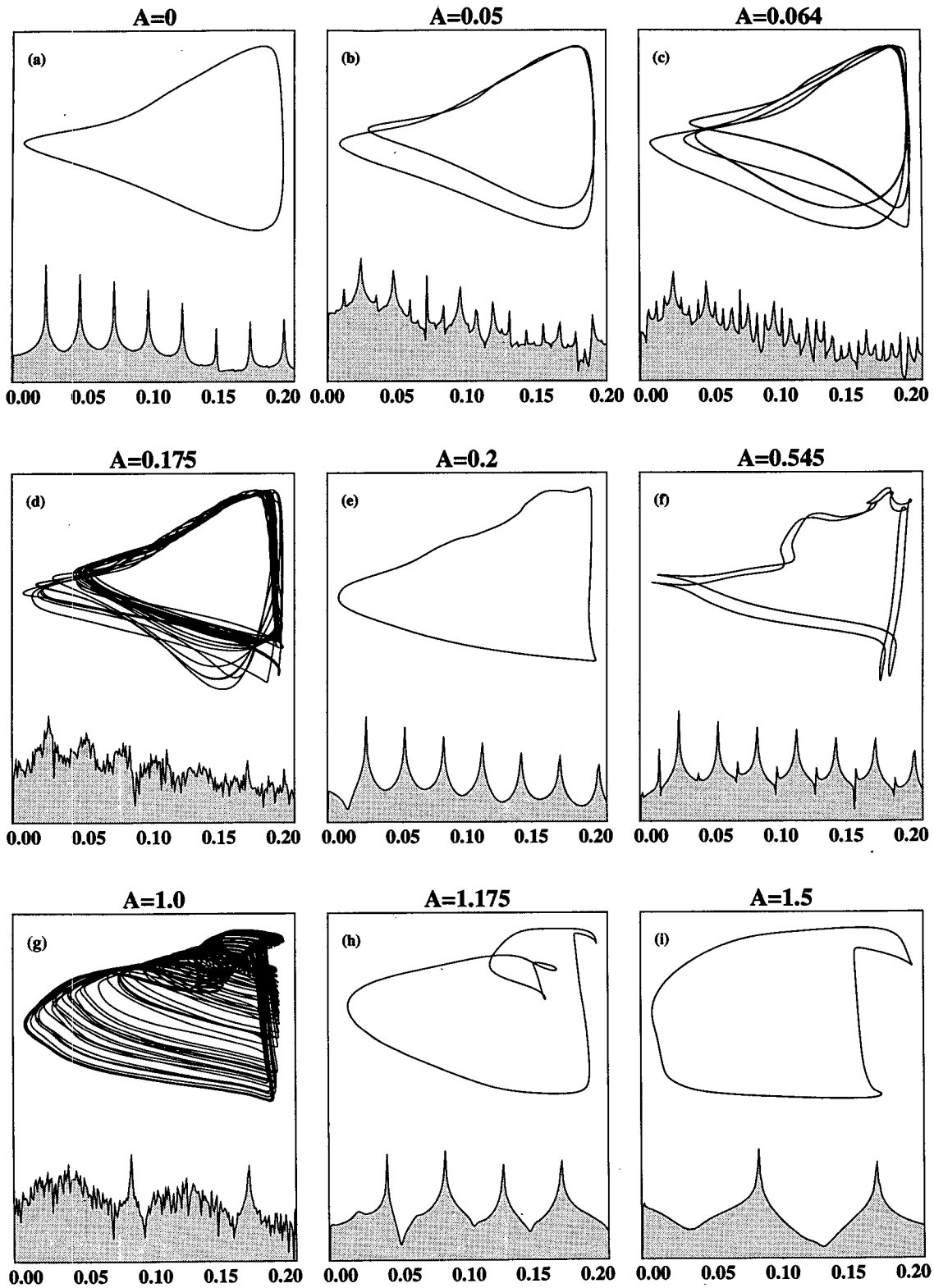

FIG. 6. Selected phase portraits (upper) and power spectra (lower) of the model SST in the eastern equatorial Pacific (0°, 120°W) for various values of the seasonal heat flux forcing amplitude A. The phase portraits are reconstructed using the method of time delay. The delayed time is determined by autocorrelation analysis. The power spectra are shown in log-linear plots and the frequency is in units of months^{-1}.

a low-order rational number of 1/3. In contrast to Figs. 5e and 6d, sharp spectral peaks with no background noise and a single period limit cycle are observed (see Figs. 5f–h and Fig. 6e).

A further increase of the forcing amplitude leads to another sequence of period doublings and eventually to chaos (Figs. 5i–q and Figs. 6f–g). The chaotic oscillations occupy a relatively wide range of $0.575 < A < 1.05$ (Figs. 5k–q). Within this large chaotic region, most SST power spectra display broadband structures and contain substantial power at low frequencies except in a few narrow windows (an example is shown in Fig. 5l) where oscillations appear to be periodic. In particular, when the forcing amplitude takes the observed value—that is, $A = 1.0$—the peaks of interannual oscillations are so broadened and the spectrum contains so much noise that it becomes nearly featureless, as in Fig. 5p. The only distinguishable peaks are at annual and semiannual frequencies that correspond to the two dominant forcing frequencies. The existence of a strange attractor at $A = 1$ is revealed by the phase portrait shown in Fig. 6g. Further analysis of the strange attractor is given in section 5a.

Beyond the large chaotic region, a frequency-locking regime appears again in the interval ($1.1 < A < 1.27$). The regular oscillations manifest themselves as sharp peaks in the power spectra (Figs. 5r–u), but the dominant frequency of interannual oscillations shifts once again from 1/4 cycle/yr in the previous frequency locking

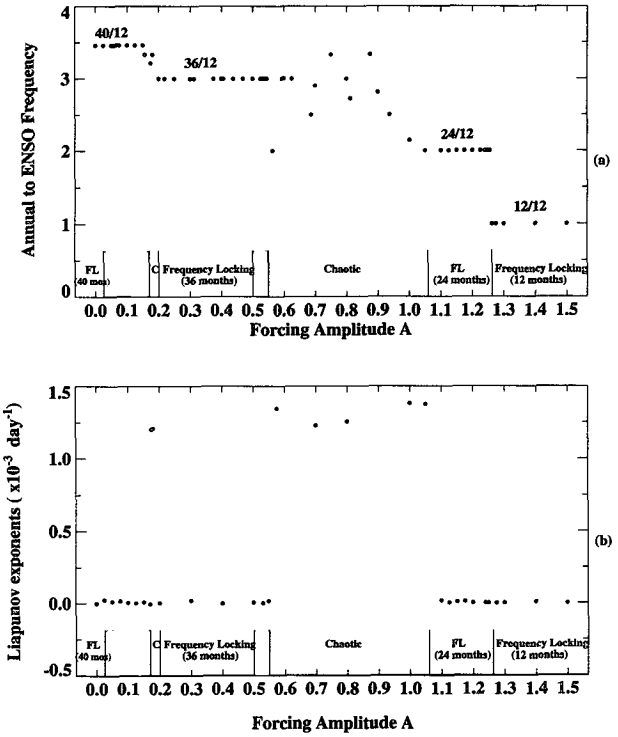

FIG. 7. (a) Ratio of frequencies of the ENSO cycle to the annual cycle in the coupled model as a function of the seasonal heat flux forcing amplitude A. Three phase-locking regimes of period of 3

The 1000-year monthly averaged SST time series were used in the calculations. The delay time which approximately corresponds to the decorrelation time of the time series varies from 2 months in strong forcing case to 5 months in the weak forcing case. The embedding dimension was taken to be approximately twice the value of the attractor dimension, which varies between 3 and 5 depending on the forcing parameter A. The results are summarized in Fig. 7b. In comparison with Fig. 7a, it is clear that Lyapunov exponents in chaotic regions are several orders of magnitude larger than those in the frequency-locking regime, indicating that the solutions in chaotic regions are much more sensitive to initial conditions than those in the frequency-locking regime. The magnitude of the exponents reflects the timescale on which the system becomes unpredictable. According to our calculation, the error-doubling time $T = (\ln 2)/K$, where K is Kolmogorov entropy and is approximately equal to the sum of all the positive Lyapunov exponents, is about 500 days under the realistic forcing conditions—that is, $A = 1$. The value is somewhat larger for the weaker forcing. It will be shown in section 5 that the error-doubling time calculated based on the positive Lyapunov exponents is consistent with the estimate from the fractal dimension analysis.

b. *Experiments of varying coupling strength in the absence of the seasonal cycle*

In the second set of experiments, the seasonally varying part of the surface heat flux forcing was completely turned off ($A = 0$) and the coupling parameter δ was varied from 0.5 to 2.0. Figure 8 displays the SST power spectra of nine different experiments with coupling parameter ranging from 0.75 to 1.83. All the power spectra exhibit multiple sharp spectral peaks with essentially no background noise, indicating regular but nonsinusoidal oscillations. A close examination further indicates that the period of the model ENSO increases continuously with the increase of the coupling strength. There appears to be no frequency locking in this case. However, the system does undergo a Hopf bifurcation at $\delta = \delta_H$, where $0.74 < \delta_H < 0.75$. Below this critical value, the coupled model has no self-sustaining oscillation. In phase space, this means the model solution changes from a fixed point to a limit cycle. This change in dynamic behavior of the model response is illustrated in Fig. 9, which shows a damped oscillation at $\delta = 0.74$ and a self-sustaining oscillation at $\delta = 0.75$.

c. *Experiments of varying coupling strength in the presence of the seasonal cycle*

In contrast to the second set of simulations, the experiments in the presence of the seasonal cycle exhibit much richer dynamic behavior of the coupled system. Figure 10 shows the SST power spectra derived from 24 different numerical experiments. The dynamic behavior of model response exhibits several stages. For extremely weak coupling strength $\delta \leq 0.5$, the coupled model "gives up" its intrinsic mode of interannual oscillations and oscillates at the forced seasonal frequency (Fig. 10a). For $0.5 < \delta < 0.94$, the coupled model experiences frequency locking and has a regular biennial oscillation (Figs. 10b–g). In the parameter regime $0.94 < \delta < 1.02$, model ENSO cycle appears to be chaotic. The chaos results from a sequence of period doubling bifurcations starting from the 2-year frequency locking as δ increases (Figs. 10h–k). Between $\delta \approx 1.03$ and $\delta \approx 1.038$, there appears to be a brief frequency-locking regime with an oscillation period of 3 years (Figs. 10l–m). Following this 3-year locking regime is a broad chaotic regime within which narrow windows of period oscillation are observed (Figs. 10n–u). Beyond $\delta = 1.25$, the coupled model is again frequency locked with the seasonal cycle with an oscillation period of 4 years (Figs. 10v–x). The frequency locking and the period doubling route to chaos observed here are very similar to those described in the first set of experiments. It is interesting to note that the coupled model response is very sensitive to changes in the coupling strength near $\delta = 1$. A small increase or decrease in the coupling strength can push the system from a chaotic regime into a 3-year or a 2-year frequency-locking regime. The high sensitivity of the response of intermediate coupled models to changes in coupling strength was also noted by Jin et al. (1994) and Tzipermen et al. (1994), although their coupled models were different from the one used here.

Finally, it is worth noting that the biennial oscillation can exist in the weakly coupled regime. As shown in the second set of experiments, in the absence of the seasonal cycle the intrinsic interannual mode of oscillation cannot be self-sustained in the coupled system when the coupling coefficient δ is below its critical value δ_H. Interestingly, even within this weakly coupled regime, there appears to be a region in the parameter space where the biennial oscillation can exist, as shown in Figs. 10b and 10c. The biennial oscillation in this weakly coupled case is apparantly excited as a subharmonic resonant response by the strong seasonal forcing. Rasmusson et al. (1990), using COADS observation, identified a particularly well-defined standing biennial oscillation, which appears as a fundamental element of ENSO variability in the low-latitude eastern Indian and western Pacific sector, tightly phase locked with the annual cycle. They suggested that the relationship between the biennial mode and the seasonal cycle is more complex than a simple modulation of the annual cycle such as proposed by Meehl (1987). Our result implies that this biennial oscillation mode could be a subharmonic resonance of the seasonal forcing rather than a self-sustaining oscillation of the coupled system.

Power Spectra of CZ–CPT Model SST

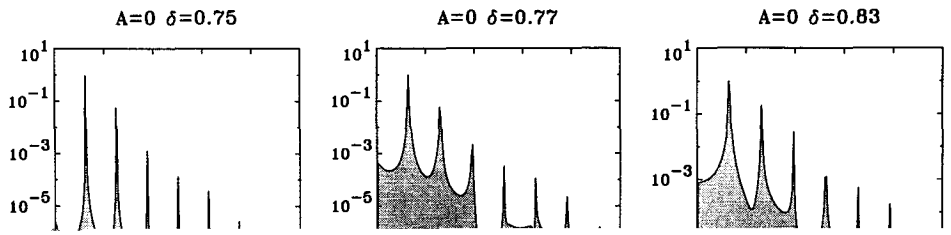

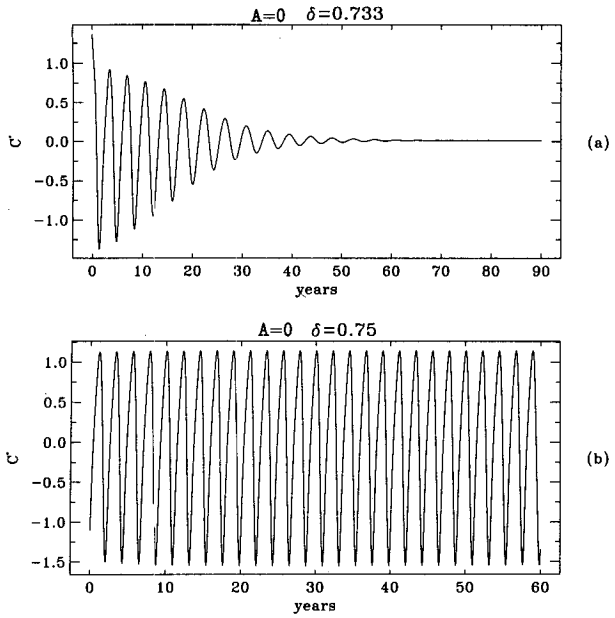

FIG. 9. Model SST anomaly time series at 120°W, 0° (a) when $A = 0$, $\delta = 0.73$ and (b) when $A = 0$, $\delta = 0.75$. For $\delta \leq 0.73$, the coupled model has no self-sustained oscillations.

time series from the control experiment ($\delta = 1$ and $A = 1$). Using "delay coordinates," an SST phase portrait is reconstructed with a delay time $\tau = 3$ months as shown in Fig. 11a. Here τ is defined as the lag time at which the autocorrelation function falls below a threshold value of 0.27. With the 3-month delay time, the 1000-year monthly time series has approximately 4000 independent data points. According to the criterion given by Eckmann and Ruelle (1992), the maximum relevant dimension that can be deduced from this

(1983b) to compute the Kolmogorov entropy K. For sufficiently large embedding dimension k, the Kolmogorov entropy K is approximately given by $K = (1/n\tau) \ln[C_k(r)/C_{k+n}(r)]$, where $C_k(r)$ is a correlation function of embedding dimension k, τ is the delay time, and the value of r should be within the linear part of the plot of $\ln C_k(r)$ versus $\ln r$. The error-doubling time $T = (\ln 2)/K$ computed based on the correlation function is about 520 days, which is consistent with the estimate from Lyapunov exponents in the previous section.

To test the significance of the result derived from the Grassberger and Procaccia algorithm, we performed a statistical hypothesis testing by redoing the dimension calculations with surrogate data. The method of surrogate data was developed by Theiler et al. (1992) to discriminate between chaos and noise from a time series. Surrogate data is generated by reprocessing the original time series so that it has the same Fourier power spectrum but has lost all of its deterministic character [see Theiler et al. (1992) for a detailed discussion]. Comparing dimensions obtained from the original time series and surrogate data can help us decide whether a model of deterministic chaos or a model of purely stochastic processes best represents the behavior of the dynamical system. Such a comparison is presented in Fig. 11c. As can be seen, the slope of the correlation function computed from surrogate data does not converge to a low dimension number as the embedding dimension increases. The range of the dimensions derived from the original time series is clearly separated from the dimensions of surrogate data, suggesting that the irregularity of the model ENSO cycle can be explained by the existence of a strange attractor with a fractal dimension of approximately 5.2. Similar analysis was performed by Tziperman et al. (1994) us-

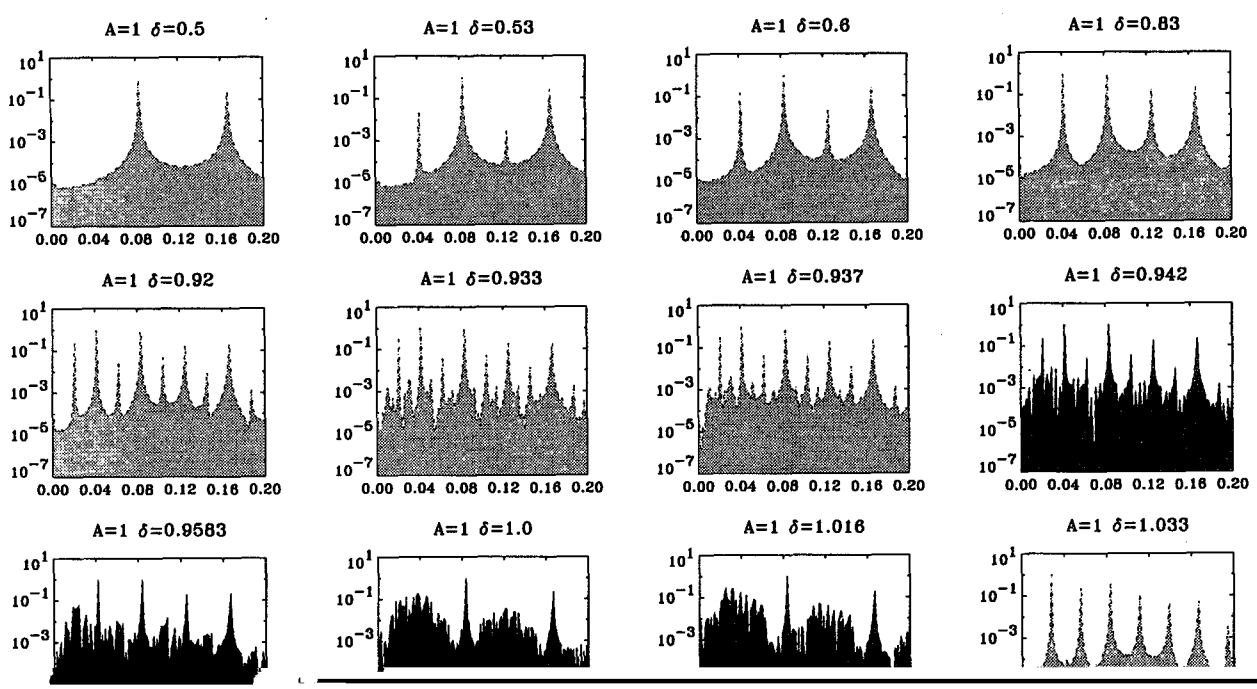
Power Spectra of CZ–CPT Model SST
A=1 δ=0.5
A=1 δ=0.53
A=1 δ=0.6
A=1 δ=0.83
A=1 δ=0.92
A=1 δ=0.933
A=1 δ=0.937
A=1 δ=0.942
A=1 δ=0.9583
A=1 δ=1.0
A=1 δ=1.016
A=1 δ=1.033
0.00 0.04 0.08 0.12 0.16 0.20

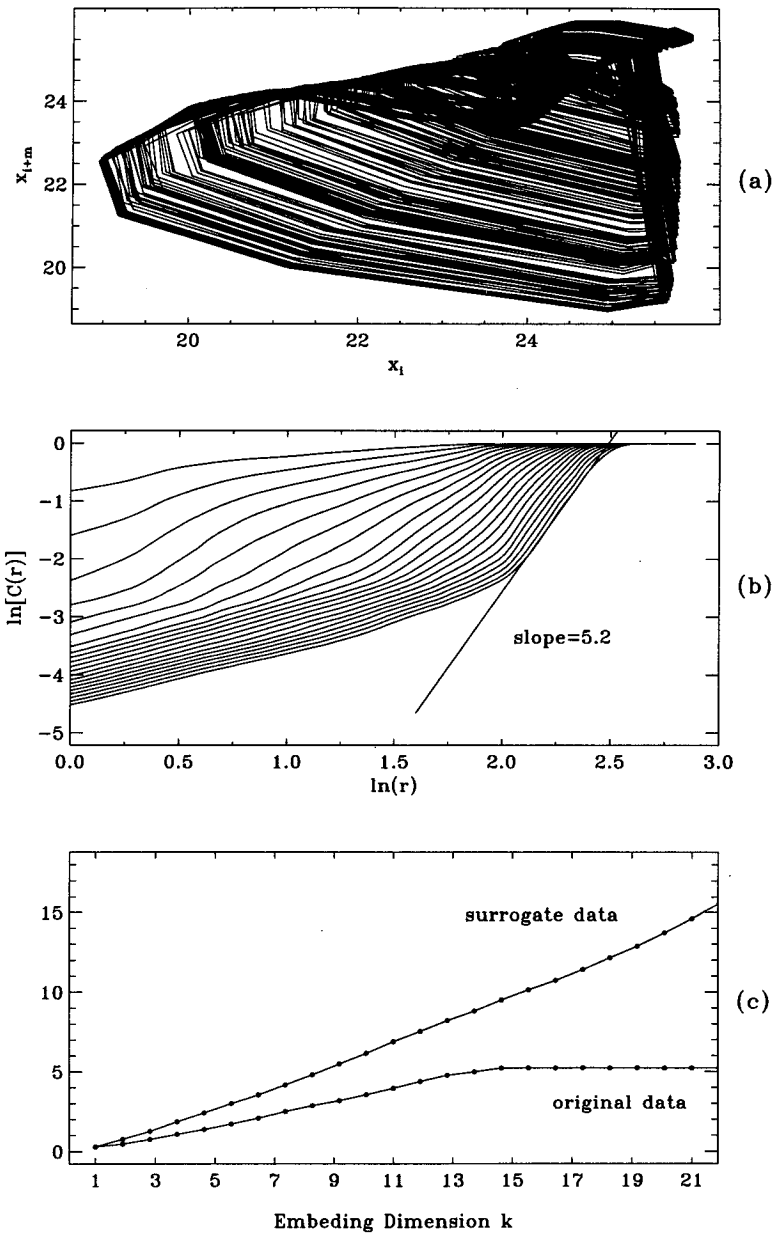

FIG. 11. (a) Phase portraits reconstructed using the 1000 years monthly SST time series at 0°, 120°W with a delay time of 3 months. (b) Logarithm of the Grassberger–Procaccia correlation function $C(r)$ as a function of the logarithm of the distance in phase space r for embedding dimensions $k = 1$ to 21 derived from the monthly mean SST time series at 0°, 120°W of the 1000-year integration of the coupled model. The fractal dimension is given by the slope of the linear segment in these curves. (c) The slope of the correction function as function of the embedding dimension k computed using both the original SST time series and "surrogate" data.

b. *Phase locking of ENSO episodes with the seasonal cycle*

As shown by Rasmusson and Carpenter (1982), observed major ENSO warm episodes exhibit a strong tendency for phase locking with the seasonal cycle in the sense that warmings in the eastern Pacific Ocean tend to occur during a particular season. To identify this phase-locking relationship from both the observed and modeled SST time series, we perform the following analysis. First, we remove the seasonal cycle from the time series by substracting the monthly climatological mean values. We then separate the positive SST anomalies from the negative ones and group them separately

according to calendar month. For each calendar month, we compute standard deviations of the positive and negative SST anomalies and ignore the data points below the standard deviations by regarding them as the "non-ENSO-year" values. Finally, we take the averages of all the positive (or negative) SST anomalies above the positive (or below the negative) standard deviation to obtain a composite of warm ENSO episodes (or cold ENSO episodes). Figure 12 illustrates warm ENSO composites derived from both the observed and modeled SST time series. The observed data were taken from the monthly mean COADS SST averaged over an area of 20° long × 8° lat centered at 120°W for the 119-year period from 1870 to 1988. This dataset was prepared by Pan and Oort and was used by Gu and Philander (1995) in their study of the secular changes of annual and interannual variability. The modeled SST time series are taken at 120°W, 0° from the first set of experiments. The dashed and solid lines in each plot show the standard deviation and the composite of ENSO warm events, respectively. Scattered dots represent monthly SST values. From Fig. 12, ENSO phase locking with the seasonal cycle is evident in the observation and in all the numerical simulations that include the seasonal cycle. The phase locking in the model occurs not only when the ENSO cycle is periodic (frequency locked) but also when it is chaotic. However, in comparison with the observation, the model ENSO cycles appear to be more tightly phase locked with the seasonal cycle and the peaks of warm episodes tend to occur in October rather than in December as shown in nature (Fig. 12a). Similar analysis for the negative SST anomalies reveals that the cold ENSO episodes in the model also exhibit a strong tendency for calendar phase locking with the peaks of cold events occurring in the same month (not shown). Such a preferred phasing with the seasonal cycle for the cold ENSO episodes, however, is less evident in nature. The fact that the model ENSO cycles have a stronger tendency for phase locking with the seasonal cycle suggests that other processes, such as stochastic forcing, in the atmosphere and oceans that have been neglected in the coupled model may also contribute to the irregularity of ENSO.

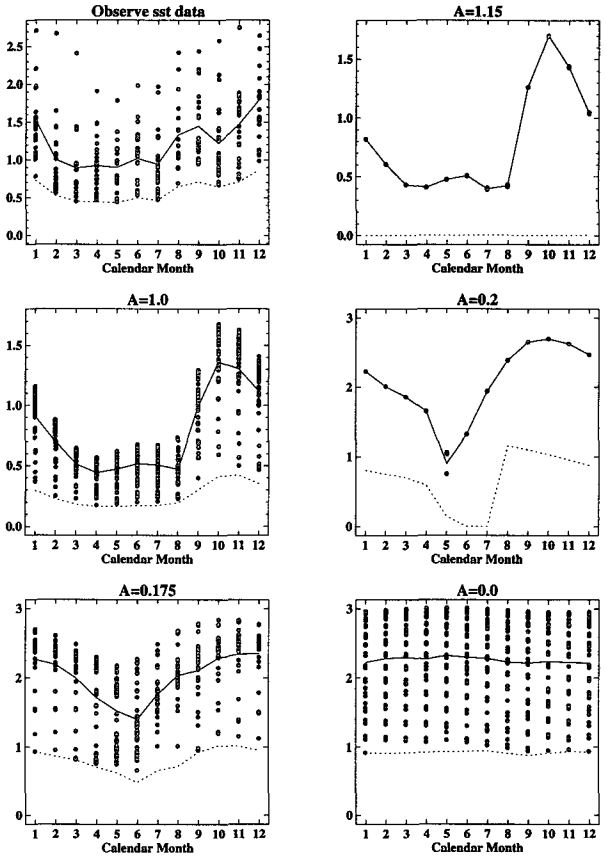

FIG. 12. Composite of warm ENSO episodes and from the 119-year observed SST time series from COADS averaged over an area of 8° lat × 20° long centered at 120°W (a) and from the model SST time series at 120°W, 0° for $A = 1.15$ (b), $A = 1.0$ (c), $A = 0.2$ (d), $A = 0.175$ (e), and $A = 0$ (f). The dashed lines indicate standard deviation for each calendar month and the solid lines show the composite warm ENSO episodes.

c. *Modulation of the seasonal cycle by the ENSO cycle*

To quantify the relationships in amplitude changes between the seasonal cycle and ENSO cycle, a Morlet wavelet transform is applied to the SST time series from the control experiment. The wavelet transform treats the time series in both time and frequency domains and can provide information about how the amplitude of a certain frequency oscillation in the time series evolves with time (Grossman 1988; Farge 1992). Gu and Philander (1995) applied the Morlet wavelet transform to analyze secular changes in the interannual variability and the seasonal cycle of selected equatorial regions over the past century. They found that not only does the amplitude of the ENSO cycle have an interdecadal variation, but also the amplitude of the seasonal cycle varies on short timescales of 2 to 5 years. In particular, they noticed that on these short timescales the changes in the seasonal cycle amplitude appear to be modulated by the interannual amplitude fluctuations in the eastern Pacific; namely, the amplitude of the seasonal cycle tends to be small during warm phase of ENSO cycle and large during cold phase. Following Gu and Philander (1994), we applied a similar wavelet transform to the SST time series at 0°, 120°W in the control experiment. For the mother wavelet, we used the Morlet wavelet $\psi(t) = e^{-i2\pi t} \exp\{-[(2\pi/K_\psi)]^2(|t|^2/2)\}$, where t is in units of a year and K_ψ is chosen to be 6 years, as suggested by Gu and Philander (1995). For a detailed discussion of the choice of mother wavelet, readers are referred to Gu and Philander (1995). The results of the wavelet

analysis are displayed in Fig. 13, which contains a 100-year segment of the SST time series at 120°W, 0° taken from the 1000-year simulation. In this figure the amplitude of the SST seasonal cycle represented by the normalized energy contained in frequency band between 1.43 yr^{-1} and 0.83 yr^{-1} is shown as the solid line. Superimposed is the interannual variation of SST (dashed line) obtained by applying a lowpass filter with a cutoff frequency of 0.63 yr^{-1} to the anomalous SST time series. It is evident from Fig. 13 that on the short timescale the maximum (minimum) amplitudes of the seasonal cycle approximately coincide with the cold (warm) ENSO episodes in the model, suggesting that the amplitude of the model seasonal cycle is regulated by the ENSO cycles. This result is consistent with the finding reported by Gu and Philander (1995) in their study of observed seasonal and interannual variability of SST. As they pointed out, the out-of-phase relation between the amplitude of seasonal and ENSO cycle is a manifestation of the influence of the interannual variations in the depth of the thermocline on the intensity of vertical entrainment process in the eastern Pacific Ocean.

6. Summary and discussion

In this study, we present a new intermediate coupled model in which total, rather than anomalous, surface winds and SST fields are coupled according to the nonlinear bulk formula. The coupled model is forced by surface heat flux primarily controlled by the annual variation of solar radiation. Coupling between total winds and SST allows the model to produce its own seasonal cycle and thus the coupled model presented here includes more complete physics than the existing intermediate anomaly models that have a fixed seasonal cycle. Numerical simulations with the observed surface heat flux forcing indicate that the model is capable of capturing essential climate variabilities on the seasonal-to-interannual timescale. Therefore, our coupled model represents the first time that the interaction between the seasonal cycle and the ENSO variability can be addressed properly because the model could be forced externally to produce both a seasonal cycle and the ENSO mode.

Model sensitivity studies demonstrate that the coupled model is not only sensitive to changes in condi-

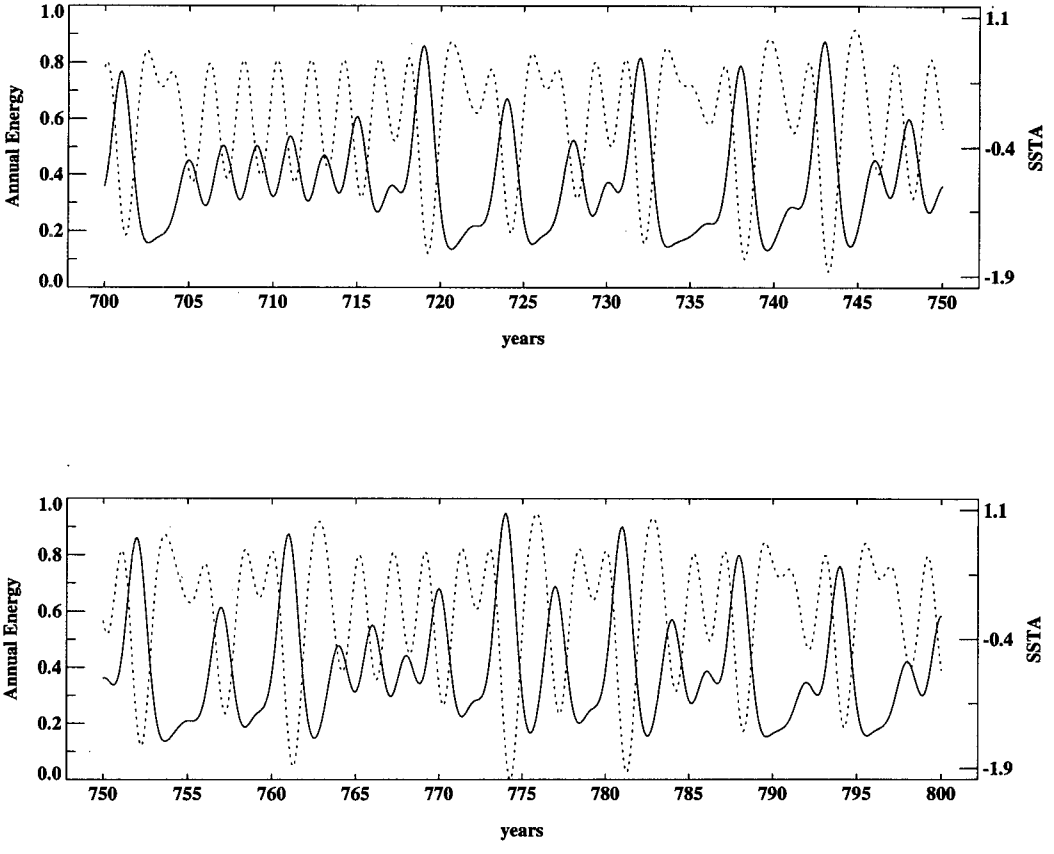

FIG. 13. Secular changes of the model SST seasonal cycle and interannual variation derived from the 1000-year simulation. The secular changes of the seasonal cycle are represented by the normalized energy of the seasonal cycle (solid line) and the SST interannual variation is obtained using a low-pass filter with a cutoff period of 19 months (dashed line). Time series shown is from year 700 to 800.

tions, such as the coupling strength of the system, that determine the internal processes, but also sensitive to changes in the external forcing condition. In particular, the coupled model exhibits much more rich dynamical behavior when the seasonal cycle is present than when it is absent. Depending on the parameter regime, the coupled system may change from a frequency-locking (periodic) state to a chaotic state or completely abandons the natural mode of oscillation for a moderate change in the coupling strength or external forcing condition. Under realistic forcing conditions, the model ENSO cycle falls into a chaotic regime sandwiched between 3-year and 2-year frequency-locking regimes. The aperiodic model response can be explained by the existence of a strange attractor with a fractal dimension of approximately 5.2. Therefore, the coupled model can be identified as a deterministic chaotic system governed by its inherent nonlinear interactions. These results contrast sharply to the results from the experiments without the seasonal cycle, which show neither frequency-locking phenomenon nor chaos. It suggests that nonlinear interactions between the forced seasonal oscillation and the intrinsic ENSO mode of oscillation are crucial for the irregular behavior of the model ENSO cycle. Our numerical experiments also reveal that a biennial oscillation can be excited by the seasonal forcing in a regime where the air–sea coupling is sufficiently weak such that self-sustaining oscillations cannot exist without the seasonal forcing. It implies that the biennial oscillation observed as a fundamental element of ENSO variability in the low-latitude eastern Indian and western Pacific sector could be a subharmonic resonant response to the seasonal forcing rather than a self-sustaining oscillation of the coupled system. This finding appears to be consistent with the observational evidence presented by Rasmusson et al. (1990), which shows that the biennial mode is tightly phase locked with the seasonal cycle. They further suggested that the understanding biennial variability seems to be intimately linked with an understanding of the seasonal cycle and it may be essential to view the seasonal cycle of the Tropics as a variable coupled ocean–atmosphere forced mode. Since monsoon circulation constitutes a major component of the seasonal cycle in the Indian Ocean–Pacific Ocean sector, a comprehensive study of the biennial oscillation requires a fully coupled global ocean–atmosphere–land model that treats monsoon trade wind systems as a unit.

Analysis of model SST time series reveals a two-way interaction between the seasonal and ENSO cycles. On the one hand, the seasonal cycle produces a strong tendency for annual phase locking of the ENSO cycles. On the other hand, the ENSO cycle significantly modulates the amplitude of the seasonal cycle. In comparison with the observation, the ENSO episodes in the model appear to be more tightly phase locked with the seasonal cycle and the peaks of the warm events occur two months earlier than those in nature. Moreover, the modulation of the seasonal cycle by the ENSO cycle in the model appears to be similar to that in observations (Gu and Philander 1995). The annual phase locking may have implications to the so-called spring break problem, which refers to the rapid decrease of the ENSO-prediction skills in coupled models during boreal spring (Latif and Graham 1992; Cane 1993). Because of the annual phase locking, the signal-to-noise ratio of ENSO during spring is usually much lower compared to the other seasons. It means that the ENSO signals are most likely to be contaminated by noises during spring, which could cause sharp decreases in model prediction skills. The physical mechanisms governing the annual phase locking are currently unclear. Also not clear is the relation between the annual phase locking and the negative correlation in amplitude changes between the seasonal cycle and ENSO. Works in progress attempt to further look into these issues and to clarify the physical processes that are responsible for producing these intimate relations between the seasonal cycle and interannual variabilities.

This study suggests that the seasonal cycle can have dual effects on interannual variabilities: on the one hand, it can introduce a degree of regularity into the ENSO cycle by producing calendar phase locking. On the other hand, it can also generate chaotic behavior in the coupled system through strong nonlinear interactions with interannual oscillations. While the role of the seasonal cycle as a fundamental pacemaker of the ENSO cycle may be widely recognized, its role in causing ENSO irregularity is highly controversial. The present study along with previous works by Jin et al. (1994), Tziperman et al. (1994), and Chang et al. (1994) have proposed that the ENSO irregularity can be viewed as a low-order chaotic process driven by the seasonal cycle. Others (Barnett and Hasselmann 1979; Graham and White 1988; Battisti and Hirst 1989; Penland and Sardeshmukh 1995) have argued that irregular recurrence of ENSO could be primarily due to stochastic processes in the coupled atmosphere–ocean system. Clearly, there is a need for further investigations to understand the relative importance of chaotic versus random processes in the evolution of ENSO. Unfortunately, identifying chaos from observed time series currently poses a very difficult task because the available instrumental record of the ENSO data is too short to be used with the techniques developed to analyze chaotic behavior of a system directly from time series. However, further understanding of the dynamic properties of the ENSO system can be gained by experimenting coupled ocean–atmosphere models of different complexity with and without random forcing. Such a modeling effort is being undertaken and the results will be presented in subsequent papers.

Recently, Tziperman et al. (1995) conducted a similar sensitivity study of the CZ model. In their study, both the coupling strength and the seasonality amplitude were also varied. Some important differences and

similarities between the results of their work and the present work are worth mentioning. For example, the CZ model was found to be chaotic in the absence of a seasonal cycle, whereas the present model is regular, and the CZ model showed no period doubling beyond the frequency-locked regimes, whereas the present model does. On the other hand, both models have no self-sustaining oscillations below some critical coupling strength; both models exhibit frequency locking and chaotic behavior in the presence of the seasonal cycle, and both models display annual phase locking of ENSO in the chaotic regime. These differences may be manifestations of the different coupling approaches in the coupled models. However, the similarities imply that nonlinear interactions between the seasonal cycle and interannual oscillation is a robust mechanism of generating ENSO irregularity in the intermediate coupled models. In general, the present study represents a more rigorous examination of the interaction between the seasonal cycle and the ENSO variability than the work by Tziperman et al. (1995) because the coupled model is forced externally to produce both a seasonal cycle and the ENSO mode and thus is more complete than the CZ model. However, it is important to point out that the ocean–atmosphere coupling in the present model is still incomplete because the thermodynamic feedbacks are excluded by specifying the latent and sensible heat fluxes in the surface forcing. These fluxes depend crucially on the air–sea boundary conditions, which ought to be predicted by the model. At present, the role of the thermodynamic feedback processes on seasonal-to-interannual variability is not clear. To address this issue, future works are needed to improve the model heat flux formulation.

This study suggests that the behavior of the coupled system may rely on a delicate balance between external forcing conditions and internal physical processes governing the natural mode of oscillation. Changes in either internal or external condition could result in different behavior of ENSO cycle. Whether our coupled ocean–atmosphere model reflects the sensitivity of the real ocean–atmosphere system is an open question that will require calculation with more realistic models, specifically coupled GCMs. A few such models are being developed and at present they behave in perplexingly different ways. Some reproduce a reasonable seasonal cycle but have practically no interannual variability. Others perform reasonably well when forced with the annual mean, but not when forced with the seasonally varying solar radiation. Our results shed light on the difficulties being encountered with these coupled GCMs. What matters may be the relative amplitudes of the interannual and seasonal oscillations. Suppose that a coupled GCM is in a parameter range where, with steady forcing, it reproduces only a weak Southern Oscillation. In that case the introduction of strong seasonal forcing could completely inhibit the interannual variations. Alternatively, if a model reproduces clouds poorly then it misrepresents the albedo of the earth and in effect misrepresents the amplitude of the seasonal forcing. In this respect the low stratus clouds off the coast of Peru and California pose a problem because they reflect a considerable amount of sunshine but are difficult to capture in models because they form in a thin layer near the surface. Thus, it is conceivable that a change in the treatment of clouds in a model could qualitatively as well as quantitatively change its behavior.

Acknowledgments. We are grateful to Dr. Eli Tziperman for his critical and constructive comments about this work and to Dr. Gu for providing us with the COADS datasets and the wavelet analysis program. This research is supported by the Climate and Global Change Program of NOAA under Grants NA16RC0462-02 and NA46GP0166. One of us (P. Chang) is also supported by the NSF Young Investigator Award OCE-9357860.

APPENDIX

Governing Equations of the Coupled Model

The governing Equations for the atmosphere are as follows (see Li and Wang 1994):

$$E_1 U - \beta y V = -\frac{\partial \phi}{\partial x} \tag{A1}$$

$$E_2 V + \beta y U = -\frac{\partial \phi}{\partial y}, \tag{A2}$$

where U, V, and $\phi = g\rho_a^{-1}P_s$ denote zonal and meridional wind components and geopotential height, P_s is the sea level pressure, E_1 and E_2 are anisotropic, latitude-dependent Rayleigh friction coefficients whose values are given in Li and Wang (1994). The sea level pressure Ps is determined from a vertically integrated hydrostatic equation for a moist hydrostatic atmosphere,

$$\ln\left(\frac{P_s}{P_u}\right) = \frac{g}{R\gamma}\ln\left[\frac{T_s}{T_s - \gamma H}\right], \tag{A3}$$

where $Pu = 100$ mb is the pressure at tropopause, the height H of the tropopause is 16.8 km, and the lapse rate γ is given by an empirical formula in terms of SST T_s; that is,

$$\gamma\ (^\circ\text{C/km}) = 10^{-3}[0.106719T_s(^\circ\text{C}) + 3.26009] + 0.05. \tag{A4}$$

The governing equations for the ocean are (see Chang 1994)

$$\frac{\partial \mathbf{u}}{\partial t} + f\mathbf{k} \times \mathbf{u} = g'\nabla h + \frac{\tau}{H} + \nu\nabla^2\mathbf{u} \tag{A5}$$

TABLE A1. Oceanic model parameters.

Symbol	Parameter	Value
g'	reduced gravity	4.17 cm s^{-2}
H_s	depth of surface mixed layer	5×10^3 cm
H	depth of thermocline	1.5×10^4 cm
r_s	Rayleigh friction in surface Ekman layer	9.26×10^{-6} s^{-1}
ν	eddy viscosity	1×10^8 cm^2 s
κ	eddy diffusivity	2×10^8 cm^2 s

$$\left(\frac{\partial h}{\partial t}\right) + H\nabla\cdot\mathbf{u} = \nu\nabla^2 h \qquad \text{(A6)}$$

$$\frac{\partial T}{\partial t} + \mathbf{u}_s\cdot\nabla T = \frac{Q}{\rho_0 C_p H_s} + \kappa\nabla^2 T - \frac{1}{H_s} w_e H(w_e)(T - T_e), \qquad \text{(A7)}$$

where the horizontal velocity in the surface mixed layer $\mathbf{u}_s$ is determined from the surface Ekman flow $\mathbf{u}_e$ and the velocity $\mathbf{u}$ is given by dynamic equations (A5)

$$\mathbf{u}_s = \mathbf{u} + \mathbf{u}_e(H - H_s)/H,$$

the Ekman flow $\mathbf{u}_e$ is given by

$$r_s u_e - f v_e = \tau_x/H_s, \quad \text{and} \quad r_s v_e + f u_e = \tau_y/H_s,$$

and the entrainment velocity w_e is determined as a divergence of the surface velocity; that is,

$$w_e = H_s\nabla\cdot\mathbf{u}_s.$$

The temperature of entrained water beneath the base of the mixed layer, T_e, is given by $T_e = (1 - \sigma)T + \sigma T_d$, where σ is an adjustable parameter taken to be 0.75 and T_d is the temperature immediately beneath the base of the mixed layer. Since the model does not predict the change of subsurface T_d, changes in T_d are assumed to be related to the changes in the model-layer depth. In this study, we use a simple linear relation $T_d = \bar{T}_{\text{sub}} + \delta\partial_z\bar{T}_{\text{sub}}(h - \bar{h})$, where $\bar{T}_{\text{sub}}$ and $\partial_z\bar{T}_{\text{sub}}$ are the observed subsurface mean temperature and its vertical derivative at 50 m, $h - \bar{h}$ is the model thermocline fluctuation from its mean value, and δ is an adjustable parameter that controls influence of thermocline fluctuation on SST and thus determines the coupling strength between the model atmosphere and ocean. The model parameters used in the coupled model experiments are listed in Table A1.

REFERENCES

Anderson, D. L. T., and J. P. McCreary, 1985: Slowly propagating disturbances in a coupled ocean–atmosphere model. *J. Atmos. Sci.*, **42,** 615–628.

Bak, P., T. Bohr, and M. H. Jensen, 1985: Mode-locking and the transition to chaos in dissipative systems. *Physica Scripta,* **T9,** 50–58.

Barnett, T. P., and K. Hasselmann, 1979: Techniques of linear prediction with application to oceanic and atmospheric fields in the tropical Pacific. *Rev. Geophys. Space Phys.,* **17,** 949–968.

——, M. Latif, N. Graham, M. Flugel, S. Pazan, and W. White, 1993: ENSO and ENSO-related predictability. Part I: Prediction of equatorial Pacific sea surface temperature with a hybrid coupled ocean–atmosphere model. *J. Climate,* **6,** 1545–1566.

Battisti, D. S., and A. C. Hirst, 1989: Interannual variability in the tropical atmosphere–ocean system: Influence of the basic state and ocean geometry. *J. Atmos. Sci.,* **46,** 1687–1712.

Cane, M. A., 1993: Tropical Pacific ENSO models: ENSO as a mode of the coupled system. *Climate System Modeling,* K. E. Trenberth, Ed., Cambridge University Press, 788 pp.

——, and S. E. Zebiak, 1985: A theory for El Niño and the Southern Oscillation. *Science,* **228,** 1084–1087.

——, and ——, 1987: Deterministic prediction of El Niño events. *Atmospheric and Oceanic Variability,* H. Cattle, Ed., Royal Meteorological Society Press, 153–182.

——, M. Munnich, and S. E. Zebiak, 1990: A study of self-excited oscillations of the tropical ocean–atmosphere system. Part I: Linear analysis. *J. Atmos. Sci.,* **47,** 1562–1577.

Chang, P., 1994: A study of the seasonal cycle of sea surface temperature in the tropical Pacific Ocean using reduced gravity models. *J. Geophys. Res.,* **99**(C4), 7725–7741.

——, and S. G. H. Philander, 1994: A coupled ocean–atmosphere instability of relevance to the seasonal cycle. *J. Atmos. Sci.,* **51,** 3627–3648.

——, B. Wang, T. Li, and L. Ji, 1994: Interactions between the seasonal cycle and the Southern Oscillation—frequency entrainment and chaos in an intermediate coupled ocean–atmosphere model. *Geophys. Res. Lett.,* **21,** 2871–2820.

Eckmann, J. P., and D. Ruelle, 1992: Ergodic theory of chaos and strange attractors. *Rev. Modern Phys.,* **57,** 617–656.

——, S. Ollifson Kamphorst, D. Ruelle, and S. Ciliberto, 1986: Lyapunov exponents from time series. *Phys. Rev.,* **34A,** 4971–4979.

Esbensen, S. K., and Y. Kushnir, 1981: The heat budget of the global ocean: An atlas based on estimates from surface marine observations. Report 29, Climate Research Institute, Oregon State University, Corvallis, OR, 27 pp.

Farge, M., 1992: Wavelet transforms and their applications to turbulence. *Ann. Rev. Fluid Mech.,* **24,** 395–457.

Graham, N. E., and W. B. White, 1988: The El Niño cycle: A natural oscillator of the Pacific Ocean–atmosphere system. *Science,* **24,** 1293–1302.

Grassberger, P., and I. Procaccia, 1983a: Characterization of strange attractors. *Phys. Rev. Lett.,* **50,** 346–349.

——, and ——, 1983b: Measuring the strangeness of strange attractors. *Physica D,* **9,** 189–208.

Grossmann, A., 1988: Wavelet transforms and edge detection. *Stochastic Processes in Physics and Engineering,* P. Blanchard, L. Streit, and M. Hazewinkel, Eds., Reidel, 415 pp.

Gu, D., and S. G. H. Philander, 1995: Secular changes of annual and interannual variability in the Tropics during the past century. *J. Climate,* **8,** 864–876.

Hense, A., 1986: On the possible existence of a stranger attractor for the Southern Oscillation. *Beitr. Phys. Atmosph.,* **60,** 34–47.

Jackson, E. A., 1990: *Perspectives of Nonlinear Dynamics.* Vol. 1. Cambridge University Press, 496 pp.

Jin, F.-F., D. Neelin, and M. Ghil, 1994: El Niño on the Devil's Staircase: Annual subharmonic steps to chaos. *Science,* **264,** 70–72.

Latif, M., and N. E. Graham, 1992: How much predictive skill is contained in the thermal structure of an OGCM. *J. Phys. Oceanogr.,* **22,** 951–962.

Lau, N. C., S. G. H. Philander, and M. J. Nath, 1992: Simulation of El Niño/Southern Oscillation phenomena with a low-resolution coupled general circulation model of the global ocean and atmosphere. *J. Climate,* **5,** 284–307.

Li, T., and B. Wang, 1994: A thermodynamic equilibrium climate model for monthly mean surface winds and precipitation over the tropical Pacific. *J. Atmos. Sci.,* **51,** 1372–1385.

Meehl, G. A., 1987: The annual cycle and interannual variability in the tropical Pacific and Indian Ocean regions. *Mon. Wea. Rev.*, **115,** 27–50.

Mitchell, T. P., and J. M. Wallace, 1992: On the annual cycle in equatorial convection and sea surface temperature. *J. Climate,* **5,** 1140–1156.

Neelin, J. D., 1989: Interannual oscillations in an ocean GCM—simple atmospheric model. *Philos. Trans. Roy. Soc. London Ser. A,* **329,** 189–205.

Pachard, N. H., J. P. Crutchfield, J. D. Farmer, and R. S. Shaw, 1980: Geometry from a time series. *Phys. Rev. Lett.,* **45,** 712–716.

Pan, Y. H., and A. H. Oort, 1990: Correlation analyses between sea surface temperature anomalies in the eastern equatorial Pacific and the World Ocean. *Climate Dyn.,* **4,** 191–205.

Penland, C., and P. D. Sardeshmukh, 1995: The optimal growth of tropical sea surface temperature anomalies. *J. Climate,* in press.

Philander, S. G. H., R. C. Pacanowski, N. C. Lau, and M. J. Nath, 1992: Simulation of ENSO with a global atmospheric GCM coupled to a high-resolution, tropical Pacific ocean GCM. *J. Climate,* **5,** 308–329.

Rasmusson, E. M., and T. H. Carpenter, 1982: Variations in tropical sea surface temperature and surface wind fields associated with the Southern Oscillation/El Niño. *Mon. Wea. Rev.,* **110,** 354–384.

——, X. Wang, and C. F. Ropelewski, 1990: The biennial component of ENSO variability. *J. Mar. Sys.,* **1,** 71–96.

Ropelewski, C. F., M. S. Halpert, and E. M. Rasmusson, 1988: Interannual variability in the tropical belt. Preprints, *Seventh Conf. on Ocean–Atmosphere Interactions,* Anaheim, CA, Amer. Meteor. Soc., 70–73.

Ruelle, R., 1990: Deterministic chaos: The science and the fiction. *Proc. Roy. Soc. London A,* **427,** 241–248.

trum from a chaotic time series. *Phys. Rev. Lett.,* **53,** 1082–1085.

Seager, R., S. E. Zebiak, and M. A. Cane, 1988: A model of the tropical Pacific sea surface temperature climatology. *J. Geophys. Res.,* **93**(C2), 1265–1280.

Suarez, M. J., and P. S. Schopf, 1988: A delayed oscillator for ENSO. *J. Atmos. Sci.,* **45,** 3283–3287.

Theiler, J., B. Galdrikian, A. Longtin, S. Eubank, and J. D. Farmer, 1992: Using surrogate data to detect nonlinearity in time series. Vol. 12, *Nonlinear Modeling and Forecasting,* M. Casdagli and S. Eubank, Eds., Addison-Wesley, 163–188.

Trenbenth, K. E., and D. J. Shea, 1987: On the evolution of the Southern Oscillation. *Mon. Wea. Rev.,* **115,** 3078–3096.

Tziperman, E., L. Stone, M. Cane, and H. Jarosh, 1994: El Niño chaos: Overlapping of resonances between the seasonal cycle and the Pacific Ocean–atmosphere oscillator. *Science,* **264,** 72–74.

——, M. A. Cane, and S. E. Zebiak, 1995: Irregularity and locking to the seasonal cycle in an ENSO-prediction model as explained by the quasi-periodicity route to chaos. *J. Atmos. Sci.,* **52,** 293–306.

Walker, G. T., and E. W. Bliss, 1932: World weather V. *Mem. Roy. Meteor. Soc.,* **4,** 53–84.

Wang, B., T. Li, and P. Chang, 1995: An intermediate model of the tropical Pacific Ocean. *J. Phys. Oceanogr.,* in press.

Wolf, A., J. B. Swift, H. L. Swinney, and J. A. Vastano, 1985: Determining Lyapunov exponents from a time series. *Physica D,* **16,** 285–317.

Zebiak, S. E., 1986: Atmospheric convergence feedback in a simple model for El Niño. *Mon. Wea. Rev.,* **114,** 1263–1271.

——, and M. A. Cane, 1987: A model El Niño–Southern Oscillation. *Mon. Wea. Rev.,* **115,** 2262–2278.

Zeng, X., R. A. Pielke, and R. Eykholt, 1992: Estimating the fractal dimension and the predictability of the atmosphere. *J. Atmos.*